On the impact of triangle shapes for boundary layer problems using high-order finite element discretization

Citation: Sun, Huafei, David L. Darmofal, and Robert Haimes. "On the Impact of Triangle Shapes for Boundary Layer Problems Using High-Order Finite Element Discretization." Journal of Computational Physics 231, no. 2 (January 2012): 541–557.

As Published: http://dx.doi.org/10.1016/j.jcp.2011.09.018

Publisher: Elsevier

Persistent URL: http://hdl.handle.net/1721.1/101266

Version: Author's final manuscript: final author's manuscript post peer review, without publisher's formatting or copy editing

On the Impact of Triangle Shapes for Boundary Layer Problems Using High-Order Finite Element Discretization

Huafei Sun, David L. Darmofal, Robert Haimes [1,2,3]

Abstract

The impact of triangle shapes, including angle sizes and aspect ratios, on accuracy and stiffness is investigated for simulations of highly anisotropic problems. The results indicate that for high-order discretizations, large angles do not have an adverse impact on solution accuracy. However, a correct aspect ratio is critical for accuracy for both linear and high-order discretizations. Large angles are also found to be not problematic for the conditioning of the linear systems arising from the discretizations. Further, when choosing preconditioning strategies, coupling strengths among elements rather than element angle sizes should be taken into account. With an appropriate preconditioner, solutions on meshes with and without large angles can be achieved within a comparable time.

Key words: Triangle shape; Large angle; Aspect ratio; High-order finite element; Anisotropic problems; ILU-factorization

1. Introduction

Many physical problems exhibit highly anisotropic behaviors, where the length scale in one direction can be several orders of magnitude smaller than in the other. To resolve these features, which often occur in thin boundary layers, wakes, or shocks, highly anisotropic elements need to be employed to improve computational efficiency.

Understanding the impact of triangle shapes can provide important guidelines for mesh generation and adaptation. While high aspect ratio meshes are important for efficiency to resolve anisotropic features, triangular elements with large angles are known to deteriorate solution quality. Babuška and Aziz demonstrated that the discretization error bound of a finite element approximation on triangular meshes grows without bound as the maximum angle of elements approaches 180° asymptotically [3]. Although this is an asymptotic result and little can be said about the impact of large angles in a non-asymptotic range, avoiding large angles leads to the development of several mesh generation algorithms, including minimum-maximum triangulations [4,15], and hybrid methods with structured meshes in the regions where high anisotropy is

[1] Doctoral candidate, Aerospace Computational Design Laboratory, Massachusetts Insititute of Technology, 77 Massachusetts Ave. 37-442, Cambridge MA, 02139, sunhu@mit.edu
[2] Professor, Aerospace Computational Design Laboratory, Massachusetts Insititute of Technology, 77 Massachusetts Ave. 33-207, Cambridge MA, 02139, darmofal@mit.edu
[3] Principal Research Engineer, Aerospace Computational Design Laboratory, Massachusetts Insititute of Technology, 77 Massachusetts Ave. 37-467, Cambridge MA, 02139, haimes@mit.edu

needed [21,22]. Both of these methods have different robustness and automation problems, especially for complex geometries, and avoiding large angles in mesh generation still remains a difficult problem.

Shewchuk conducted a comprehensive study on triangle shapes for linear finite elements [34]. He concluded that the triangle shape that leads to the best accuracy in terms of the H^1-seminorm of interpolation error is one with an aspect ratio equal to the ratio $\bar{\kappa}$ of the maximum and minimum singular values of the solution Hessian but without large angles. However, he also demonstrated that this so-called "superaccuracy" is very fragile as the elements have to align *precisely* with the singular vectors of the Hessian, and so he suggested that generating triangles with an intermediate aspect ratio of $\sqrt{\bar{\kappa}}$ but possibly with large angles is a more realistic goal for anisotropic mesh generation. Also, Rippa showed in his work that this aspect ratio is optimal for the L^p-norm of the interpolation error for $1 \leq p < \infty$ [29]. Although these results provide good insight into what an optimal triangle shape should be, their analysis is limited to linear elements. Recently, Cao developed an interpolation error bound involving anisotropic features of high-order derivatives, and proposed an optimal Riemannian metric for high-order interpolations [10,11]. However, the impact of large angles is still unclear for high-order discretizations of highly anisotropic problems, and further, discretization errors can be much smaller than interpolation errors when large angles are present as argued for linear finite elements in [1]. If high-order discretizations are not sensitive to element angles, then large angles introduced by a Delaunay triangulation in a stretched space [8,13] would not be problematic.

Another important aspect of numerical simulation is the solution efficiency of the linear system arising from the discretization applied. Many have investigated the relationship between mesh quality (e.g. element angle size) and the condition number of the stiffness matrix arising from a standard Galerkin approach for a self-adjoint elliptic problem. For example, Shewchuk derived a bound on the stiffness matrix condition number for standard linear finite element [34], and recently in the work of Du *et al.* [14], a refined bound was derived for a high-order finite element. However, little can be inferred from their work when convection terms are present, which make the stiffness matrix non-symmetric. Further, although stiffness matrix conditioning is important for the efficiency of iterative linear solvers, investigating preconditioning strategies for meshes with different geometric properties has a more practical value since for many applications, only the preconditioned systems are tractable.

In this paper, the impact of large angles and element aspect ratios will be studied for boundary layer problems using high-order discretizations. Both solution accuracy and conditioning of the discretized system will be investigated when large angles are present. Results show that using a high-order discretization, the same accuracy can be achieved at similar degrees of freedom for both large-angle and right-angle triangulations. However, a correct aspect ratio is critical for accuracy. It is also found that the two mentioned triangulations have similar linear conditioning, but solution schemes for these two should be different as they involve different couplings among elements. Incomplete LU factorization, being a popular preconditioning scheme, is investigated for effectiveness on both triangulations.

This paper is organized as follows. Section 2 describes the discretization and the solution scheme applied. Sections 3 and 4 present the model problems and the meshes considered, including large-angle elements and right-angle elements. Section 5 studies the discretization errors on these meshes, and Section 6 studies conditioning of the linear systems arising from these meshes.

2. Discretization and Solution Method

2.1. *Discontinuous Galerkin Discretization*

Let $\Omega \in \mathbb{R}^d$ be an open, bounded domain in a $d-$dimensional space. A general steady state conservation law in the domain, Ω, expressed in the strong form is given by

$$\nabla \cdot \mathcal{F}^i(\mathbf{u}) - \nabla \cdot \mathcal{F}^v(\mathbf{u}, \nabla \mathbf{u}) = \mathcal{S}(\mathbf{x}), \text{ in } \Omega, \tag{1}$$

where $\mathbf{u}(\mathbf{x}) : \mathbb{R}^d \to \mathbb{R}^m$ is the $m-$state solution vector. The inviscid flux $\mathcal{F}^i(\mathbf{u}) : \mathbb{R}^m \to \mathbb{R}^{m \times d}$, the viscous flux $\mathcal{F}^v(\mathbf{u}, \nabla \mathbf{u}) : \mathbb{R}^m \times \mathbb{R}^{m \times d} \to \mathbb{R}^{m \times d}$, and the source term $S(\mathbf{x}) : \mathbb{R}^d \to \mathbb{R}^m$ characterize the governing equation to be solved.

The discretization of Eq. (1) is carried out using a Discontinuous Galerkin (DG) method on triangular meshes. Let $\mathcal{T}_H$ be a triangulation of the domain Ω with non-overlapping elements, κ, such that $\bar{\Omega} = \bigcup_{\kappa \in \mathcal{T}_H} \bar{\kappa}$. Also, define a function space $\mathcal{V}_H^k$ by

$$\mathcal{V}_H^k \equiv \{\mathbf{v} \in \left(L^2(\Omega)\right)^m : \mathbf{v}|_\kappa \in (\mathcal{P}^k(\kappa))^m, \forall \kappa \in \mathcal{T}_H\}, \tag{2}$$

where $\mathcal{P}^k(\kappa)$ denotes the space of the k-th order polynomials on κ. Multiplying Eq. (1) by a test function, $\mathbf{v}_H \in \mathcal{V}_H^k$, and integrating by parts over all elements leads to the weak formulation of the conservation law, which reads as follows: find $\mathbf{u}_H(\cdot) \in \mathcal{V}_H^k$ such that

$$\mathcal{R}_H(\mathbf{u}_H, \mathbf{v}_H) = 0, \ \forall \mathbf{v}_H \in \mathcal{V}_H^k, \tag{3}$$

where the semi-linear weighted residual (linear in the second argument) is given by

$$\mathcal{R}_H(\mathbf{u}_H, \mathbf{v}_H) = \sum_\kappa \left[\mathbb{E}_\kappa(\mathbf{u}_H, \mathbf{v}_H) + \mathbb{V}_\kappa(\mathbf{u}_H, \mathbf{v}_H) + \mathbb{S}_\kappa(\mathbf{v}_H)\right],$$

and $\mathbb{E}_\kappa(\mathbf{u}_H, \mathbf{v}_H)$, $\mathbb{V}_\kappa(\mathbf{u}_H, \mathbf{v}_H)$, and $\mathbb{S}_\kappa(\mathbf{v}_H)$ denote the contributions of the inviscid, viscous, and source terms, respectively. Specifically, Roe's numerical flux function [30] is used for the inviscid discretization, $\mathbb{E}_\kappa(\mathbf{u}_H, \mathbf{v}_H)$. The viscous flux contribution, $\mathbb{V}_\kappa(\mathbf{u}_H, \mathbf{v}_H)$, is discretized according to the second form of Bassi and Rebay (BR2) [5], which is dual consistent and requires only the nearest neighbor coupling. Further details on the discretization of the viscous term can be found in [18]. The discretization of the source term is given by $\mathbb{S}_\kappa(\mathbf{v}_H) \equiv -\int_\kappa \mathbf{v}_H^T \mathcal{S}(\mathbf{x}) d\mathbf{x}$. Boundary conditions are enforced weakly by appropriately setting the numerical flux on the domain boundaries. The boundary treatment for the Navier-Stokes equations can be found in [25].

To obtain the discrete form of the governing equation, a basis for the function space, $\mathcal{V}_H^k$, is chosen. Denote this basis by $\{\boldsymbol{\phi}_i\}$ for $i = 1, ..., N$, and let $\mathbf{U}_H \in \mathbb{R}^N$ be the vector of expansion coefficients for the solution $\mathbf{u}_H \in \mathcal{V}_H^k$, that is, $\mathbf{u}_H = \sum_{i=1}^N \mathbf{U}_{Hi} \boldsymbol{\phi}_i(\mathbf{x})$. Then the discrete form of the weak formulation in Eq. (3) can be written as a system of algebraic equations: find $\mathbf{U}_H$ such that

$$\mathbf{R}_H(\mathbf{U}_H) = 0, \tag{4}$$

where $\mathbf{R}_H(\mathbf{U}_H)$ is the discrete residual vector such that $\mathbf{R}_H(\mathbf{U}_H)_i = \mathcal{R}_H(\mathbf{u}_H, \boldsymbol{\phi}_i)$.

2.2. *Linear Solution Method*

The system defined in Eq. (4) is solved using Newton's method, where the solution vector at the $n+1$st iteration is given by

$$\mathbf{U}_H^{n+1} = \mathbf{U}_H^n - \left(\left.\frac{\partial \mathbf{R}_H}{\partial \mathbf{U}_H}\right|_{\mathbf{U}_H^n}\right)^{-1} \mathbf{R}_H(\mathbf{U}_H^n).$$

This requires at each iteration the solution to the linear system $\mathbf{K}\mathbf{x} = \mathbf{b}$, where

$$\mathbf{K} \equiv \left.\frac{\partial \mathbf{R}_H}{\partial \mathbf{U}_H}\right|_{\mathbf{U}_H^n}, \quad \mathbf{x} \equiv \Delta \mathbf{U}_H^n, \quad \mathbf{b} \equiv -\mathbf{R}_H(\mathbf{U}_H^n), \tag{5}$$

The matrix $\mathbf{K}$ is referred to as the Jacobian matrix. In the implementation of solving Eq. (4), a pseudo-time stepping is applied in order to improve the solver robustness. The time step is raised to essentially infinite value as the solution converges to steady state, at which the linear system involved is the same as Eq. (5). For the DG discretization presented, the Jacobian matrix has a sparse block-structure with N_e block rows, where N_e is the number of elements in the computational domain. Each block has a size of $n_b \times n_b$, where n_b is the number of degrees of freedom in one element. Each block row has a non-zero diagonal block, which corresponds to the coupling between degrees of freedom within one element. In addition, because the BR2 scheme requires only the nearest neighbor coupling [5], each block row of the Jacobian matrix also involves n_f off-diagonal blocks, where n_f is the number of faces per element ($n_f = 3$ for 2D).

For many problems of interest, the Jacobian matrix can be large, and iterative methods are used to solve the linear system given in Eq. (5). More specifically, a restarted GMRES algorithm [33,32] is applied in this work. To improve the convergence of the GMRES algorithm, a preconditioner must be applied. In this work, the preconditioner considered is a dual threshold incomplete LU factorization [31], ILUT(p,τ), where p is the number of allowed fill-in's per row, and τ is the fill-in drop threshold. Since the Jacobian matrix has a block structure, ILUT(p,τ) is implemented in a block form, where the Frobenius norm is used to measure the contribution of a block. The standard ILU(0), being a particular case of ILUT(p,τ) with $p = 0$ and $\tau \to \infty$, is also considered in this study and implemented in a block form.

The efficiency of incomplete factorization is highly dependent on the ordering of unknowns, especially for a non-symmetric system [6]. The reordering scheme used in this work is the Minimum Discarded Fill (MDF) method, where the element that produces the least discarded fill-in is ordered first and the process is repeated in a greedy manner. This method was presented by D'Azevdo *et al.* [12], and modified for a block matrix and reported to work well with ILU(0) in a DG context [28]. For the block form of the MDF algorithm, each block of the matrix is reduced to a scalar using the Frobenius norm, and the reordering is based on the reduced scalar matrix.

3. Model Problems

To study the impact of large angles and aspect ratios, a thin boundary layer case is used for this study, and the governing equations considered include the advection-diffusion equation and the Navier-Stokes equations, both of which have the form of the conservation law given in Eq. (1).

3.1. *Advection-Diffusion Equation*

The advection-diffusion equation has its inviscid and viscous fluxes defined as $\mathcal{F}^i \equiv \boldsymbol{\beta} u$ and $\mathcal{F}^v \equiv \bar{\bar{\mu}} \cdot \nabla u$, respectively, where $\boldsymbol{\beta}$ is the advection velocity and $\bar{\bar{\mu}}$ is the diffusivity tensor. When $\bar{\bar{\mu}}$ is isotropic, its notation is replaced by a scalar μ.

For the anisotropic problem considered in this work, the convection velocity is uniform and horizontal with a unit magnitude, and a diffusivity of $\mu = 10^{-8}$ is introduced. The computational domain is a rectangular box of $[0.05, 1.05] \times [0, 0.001]$. A source term is added such that the exact solution to this problem has a form of

$$u = 1 - e^{\frac{-y}{\sqrt{c\mu x}}}, \tag{6}$$

with $c = 0.59$. This solution is shown in Fig. 1 and resembles a thin boundary layer growing with $\sqrt{x}$ along the bottom wall. It has a thickness of $\delta_{0.99} = 8 \times 10^{-5}$ at the inflow and 3.6×10^{-4} at the outflow. Note that the leading edge of the boundary layer is not included in the computational domain.

3.2. *Navier-Stokes Equations*

For the compressible Navier-Stokes equations, the conservative state vector is $\mathbf{u} = [\rho, \rho\boldsymbol{v}^T, \rho E]^T$, where ρ is density, $\boldsymbol{v} = [u, v]^T$ is velocity vector, and E is specific total internal energy. The inviscid and viscous fluxes, $\mathcal{F}^i$ and $\mathcal{F}^v$, are given such that Eq. (1) represents a compact notation for the conservation of mass, momentum, and energy. In addition, the ideal gas law is assumed. A source term is created to make an exact solution of $\rho, P = \text{const}$, $v = 0$, and u given by Eq. (6), with $Re = 10^8$ and $M_\infty = 0.1$. The computational domain is the same as for the case of the advection-diffusion equation.

4. Meshes

As previously cited, a realistic goal for anisotropic meshing for linear elements is to generate triangles with an aspect ratio of $\sqrt{\bar{\kappa}}$, where $\bar{\kappa} \equiv \sigma_{\max}/\sigma_{\min}$ and the σ's are the singular values of the solution Hessian [34].

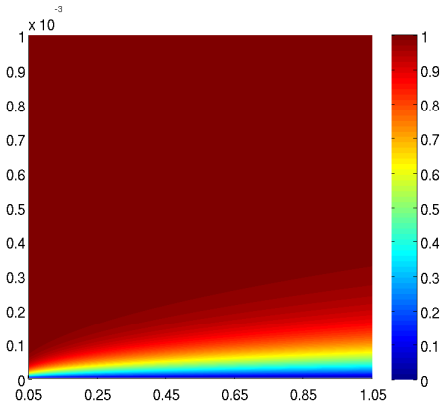

Fig. 1. Exact solution of u given in Eq. (6)

Also, at this aspect ratio, angle size is not critical for solution accuracy [34]. In fact, this value is the target aspect ratio in many anisotropic adaptation schemes for linear discretizations [27,37,20,13], in which interpolation errors are equidistributed in all directions. In this paper, this aspect ratio is used as a guideline for the meshes considered, and the element orientation is decided based on the angle θ of the singular vectors of the Hessian matrix. Further, for high-order schemes to achieve equidistribution of interpolation errors, Fidkowski proposed an aspect ratio given by

$$\mathcal{AR} = \left(\frac{u^{(k+1)}_{\mathbf{e_1}}}{u^{(k+1)}_{\mathbf{e_2}}} \right)^{1/(k+1)}, \tag{7}$$

where k is the interpolation order, $u^{(k+1)}_{\mathbf{e}}$ represents the $k+1$st derivative of u along the direction $\mathbf{e}$, $\mathbf{e}_1$ is the direction of maximum $k+1$st derivative, and $\mathbf{e}_2$, the direction orthogonal to $\mathbf{e}_1$ [17]. In fact, this is also similar to the optimal aspect ratio for high-order interpolations proposed by Cao [11].

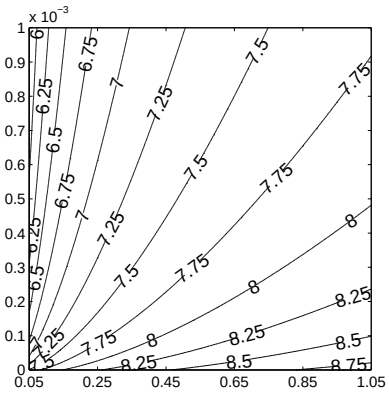

Fig. 2. $\log_{10}(\sigma_{\max}/\sigma_{\min})$ of u in Eq. (6)

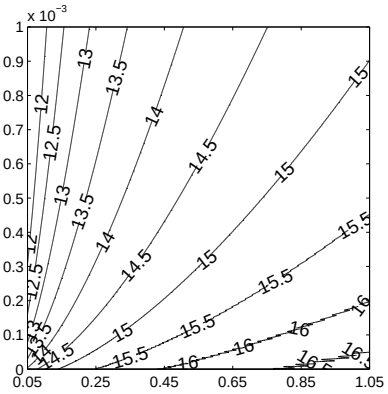

Fig. 3. $\log_{10}(u^{(4)}_{\mathbf{e_1}}/u^{(4)}_{\mathbf{e_2}})$ of u in Eq. (6)

Figure 2 shows the ratio $\bar{\kappa}$ of the solution considered in Eq. (6). Along the bottom wall, which will be the main source of discretization error, $\bar{\kappa}$ is about 10^8, so an aspect ratio of $\mathcal{AR} \approx 10^4$ might be expected to result in a high-quality solution for linear elements. Three different aspect ratios are considered in this work: 10^3, 10^4, and 10^5. Also, for the solution considered, θ is essentially zero everywhere in the computational domain, and has an average of 0.01° and a maximum value of 0.14°. This indicates that the major axes of elements should be aligned horizontally. In addition, Fig. 3 shows the ratio $u^{(4)}_{\mathbf{e_1}}/u^{(4)}_{\mathbf{e_2}}$, where $\mathbf{e}_1$ and $\mathbf{e}_2$ are defined as in Eq. (7). As shown, this ratio is about 10^{16} along the bottom wall. This indicates that equidistribution of

interpolation error in all directions leads to an aspect ratio of about $\mathcal{AR} \approx 10^4$ for an interpolation order of $k = 3$ according to Eq. (7).

To study the impact of large angles, elements with angles close to 180° (obtuse triangles) are compared with right-angle elements (acute triangles). Figure 4 shows the meshes of these two kinds of triangles. Note the y-axis is rescaled only for the convenience of visualization, so in the physical domain, each of the obtuse triangles has one angle of about 180°, and each of the acute triangles has essentially two angles of about 90°. For the aspect ratio of 10^4, the large angle in the obtuse triangles is 179.9771°.

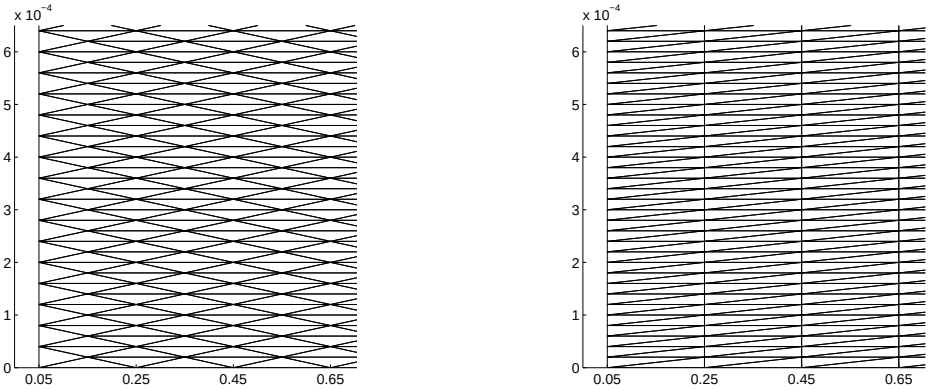

(a) Obtuse, one 180°-angle

(b) Acute, two 90°-angles

Fig. 4. Obtuse and acute meshes

5. Discretization Error

An error convergence study is conducted for the advection-diffusion equation and the Navier-Stokes equations on the meshes of all aspect ratios considered. The L^2 error and the error of a selected output are used to assess the solution quality on these meshes. For the advection-diffusion problem, the error of the heat flux across the bottom wall is measured. This output is given by

$$J = \int_{\text{bottom wall}} \mu \frac{\partial u}{\partial y} dx. \tag{8}$$

For the Navier-Stokes equations, the chosen output of interest is the drag along the bottom wall, which is also given by Eq. (8) for the model problem considered. The output is evaluated in a dual-consistent manner, and can exhibit a better convergence rate than the interpolation error of the finite element solution [19,23]. Also, the L^2 errors are normalized by the L^2 norm of the true solution, that is,

$$\mathcal{E} \equiv \frac{\|e\|_{L^2(\Omega)}}{\|u\|_{L^2(\Omega)}},$$

where $e \equiv u - u_h$, u is the exact solution as in Eq. (6), and u_h is the numerical solution from the DG discretization. The output errors are normalized by the true output value. For all cases, solution polynomial degrees of $k = 1$ and $k = 3$ are considered.

In this section, it will be demonstrated that using a high-order solution scheme, the maximum element angle size has little impact on accuracy, and such a scheme also leads to a lower error per degree of freedom. However, aspect ratio is a key factor for accuracy, for both linear and high-order solutions and for both acute and obtuse elements.

5.1. *Advection-Diffusion Equation*

The normalized L^2 errors for the acute and obtuse meshes of different aspect ratios are shown in Fig. 5, where N is the total number of elements. The adverse impact of large angles is apparent only for $\mathcal{AR} = 10^5$ for both solution orders. However, this impact appears smaller for the high-order solutions. In fact, for the high-order solutions, the difference between the acute and obtuse meshes is minor for any aspect ratio. Note the error on obtuse meshes at $\mathcal{AR} = 10^5$ for $k = 1$ is still pre-asymptotic and will exhibit a convergence rate of 2 as the mesh is uniformly refined further. As for the impact of aspect ratio, an aspect ratio of $\mathcal{AR} = 10^4$ generally leads to the lowest error at a given DOF for both shapes and for both solution orders. For the linear solutions, while the solution quality degrades slightly when the aspect ratio changes from 10^4 to 10^3, the degradation is more severe for $\mathcal{AR} = 10^5$. For the high-order solutions, the aspect ratios of 10^3 and 10^4 lead to very similar errors, but $\mathcal{AR} = 10^5$ results in a significantly higher error. In short, while the impact of aspect ratios on solution accuracy is critical, the impact of large angles is minor for high-order schemes.

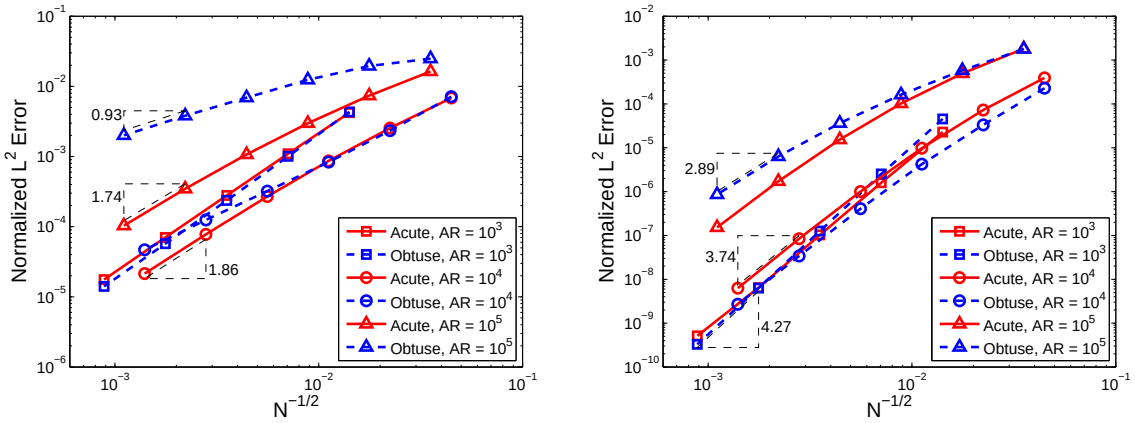

(a) Solution Order of $k = 1$

(b) Solution Order of $k = 3$

Fig. 5. Normalized L^2 error for the advection-diffusion problem. Note the different scales of y-axis in the two plots.

These results can be in fact justified from an analysis of H^1 semi-norm of interpolation errors, $|e_I|_{H^1}$, where $e_I \equiv u - u_I$ and u_I is a continuous interpolant of u. In fact, through the Aubin-Nitsche duality argument, the L^2 error of the DG discretized solution, $\|e\|_{L^2}$, is bounded by the energy norm of the error, $\|e\|_E$, within some constant. For the current DG discretization scheme, $\|e\|_E$ is further bounded by $|e_I|_{H^1}$, within some constant. Detailed derivations can be found in [2].

For linear interpolations, Shewchuk derived an error bound for $|e_I|_{H^1}$ in terms of element geometric features in [34], and showed that this error bound is sensitive to maximum angle size only at an aspect ratio much larger than $\sqrt{\bar{\kappa}} \equiv \sqrt{\sigma_{\max}/\sigma_{\min}}$ of solution Hessian, which is about 10^4 for the model problem considered in this work. Similar conclusion was also drawn in [9], and this justifies what is observed in Fig. 5 for the linear solutions. For high-order interpolations, Cao derived an error expression for a quadratic interpolation of cubic functions in a triangle centered at origin [10]. Although the impact of large angles is difficult to directly deduce from the expression, which involves rather complicated interactions with element geometric features, his numerical results led to the conclusion that large angles have impact only at an aspect ratio larger than his derived optimal value, which is similar to Eq. (7). This is consistent with the high-order results in Fig. 5. The conclusion from Fig. 5 that the impact of large angles is smaller for high-order solutions is less obvious from the analysis in the cited literatures. However, comparing the analysis of linear interpolations in [34,9] with the numerical results of quadratic interpolations in [10] can lead to the same conclusion for $|e_I|_{H^1}$.

The optimality of the aspect ratio of $\mathcal{AR} = 10^4$ can also be justified by interpolation theory for $|e_I|_{H^1}$. This aspect ratio corresponds to $\sqrt{\bar{\kappa}}$ and also Eq. (7) for the fourth-derivatives. Its optimality for linear

and high-order interpolations can be deduced from the analysis in [34,9,11]. Note for linear acute elements, although the optimal aspect ratio is $\bar{\kappa}$, this optimality is very sensitive to the alignment [34,9]. For the amount of misalignment in the current problem described in Section 3, the optimal aspect ratio will be close to $\sqrt{\bar{\kappa}}$.

Figure 6 shows the normalized heat flux error for the acute and obtuse meshes. The results lead to a similar conclusion to what was observed for the L^2 error, where only the linear solutions are susceptible to large angles; that is, the difference between the two element shapes is less pronounced for high-order solutions than linear solutions. However, a correct aspect ratio is critical for controlling the error level. While the best aspect ratio is $\mathcal{AR} = 10^4$ for both element shapes and for both interpolation orders, one important difference compared to the results of L^2 error is that $\mathcal{AR} = 10^4$ is considerably better than both $\mathcal{AR} = 10^3$ and 10^5 for linear elements. Also, note that the error reaches machine precision as the meshes are refined for the high-order solutions.

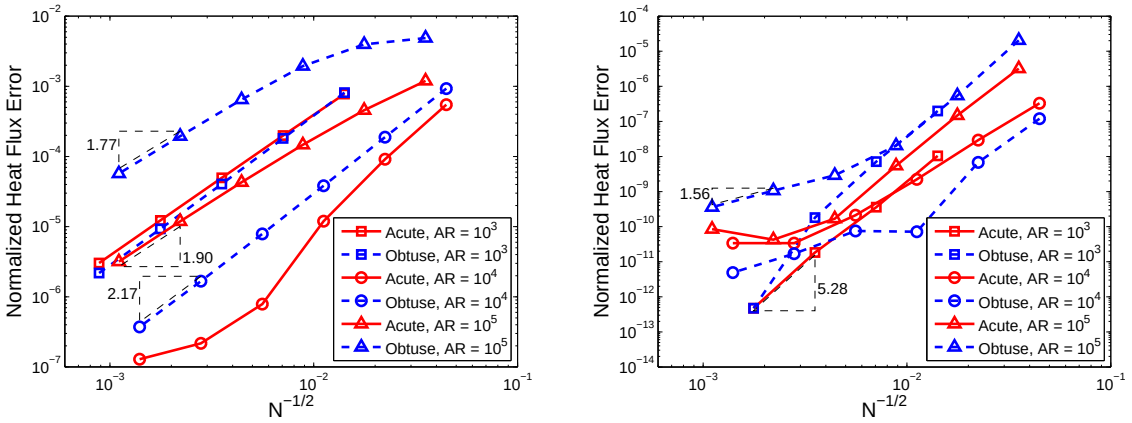

(a) Solution Order of $k = 1$

(b) Solution Order of $k = 3$

Fig. 6. Normalized heat flux error for the advection-diffusion problem

One question that naturally arises is whether these results are only observed under the DG discretization applied, or if they are a more general property of the triangulation. Consider the L^2 projection of the exact solution, denoted by $\mathbf{u}_{L^2}$, and denote the DG solution by $\mathbf{u}_{DG}$. Recall from Fig. 5 for the DG solution $\mathbf{u}_{DG}$, the difference between the acute and obtuse triangles is pronounced at only $\mathcal{AR} = 10^5$, especially for $k = 1$. In contrast, this difference is minor for $\mathbf{u}_{L^2}$ for both $k = 1$ and $k = 3$, as shown in Fig. 7, which compares the L^2 error of $\mathbf{u}_{L^2}$ and $\mathbf{u}_{DG}$ at $\mathcal{AR} = 10^5$. In fact, it is found that $\mathbf{u}_{L^2}$ is not sensitive to element angle size for all the aspect ratios considered. In other words, the approximabilities of the acute and obtuse meshes in L^2 norm are essentially the same. This indicates the possibility of designing a discretization scheme whose L^2 error is less sensitive to element angle size, for example, a scheme with its energy norm being equivalent to the L^2 norm. In contrast, for a scheme that has the L^2 error bounded by H^1 interpolation errors within some constant, e.g. the DG scheme used in this paper or a standard Galerkin scheme, the conclusions drawn from Fig. 5 can still be valid.

5.2. *Navier-Stokes Equations*

Figure 8 shows the convergence of the normalized L^2 error of ρu for the Navier-Stokes equations. The conclusion drawn is very similar to that of the L^2 error for the advection-diffusion case. For the linear solutions, an aspect ratio of $\mathcal{AR} = 10^4$ generally leads to the lowest error at a given DOF for both element shapes, and the degradation of solution quality is more severe for $\mathcal{AR} = 10^5$ than for $\mathcal{AR} = 10^3$. Also, the impact of large angles is more pronounced for $\mathcal{AR} = 10^5$ than other aspect ratios. For the high-order solutions,

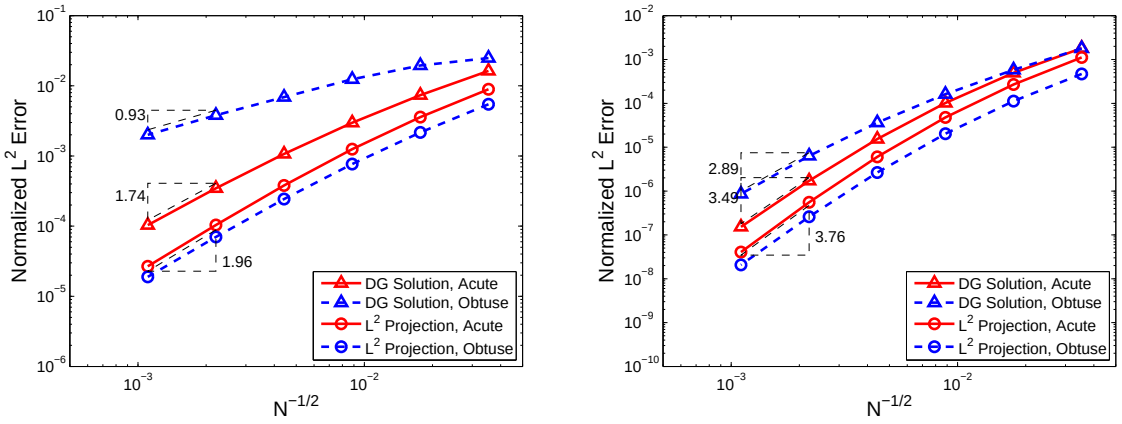

(a) Solution Order of $k = 1$ (b) Solution Order of $k = 3$

Fig. 7. Normalized L^2 error of L^2 projection of exact solution and DG solution at $\mathcal{AR} = 10^5$

the aspect ratios of 10^4 and 10^3 lead to very similar errors, but $\mathcal{AR} = 10^5$ results in a significantly higher error. However, the difference between the two triangle shapes is minor for any aspect ratio.

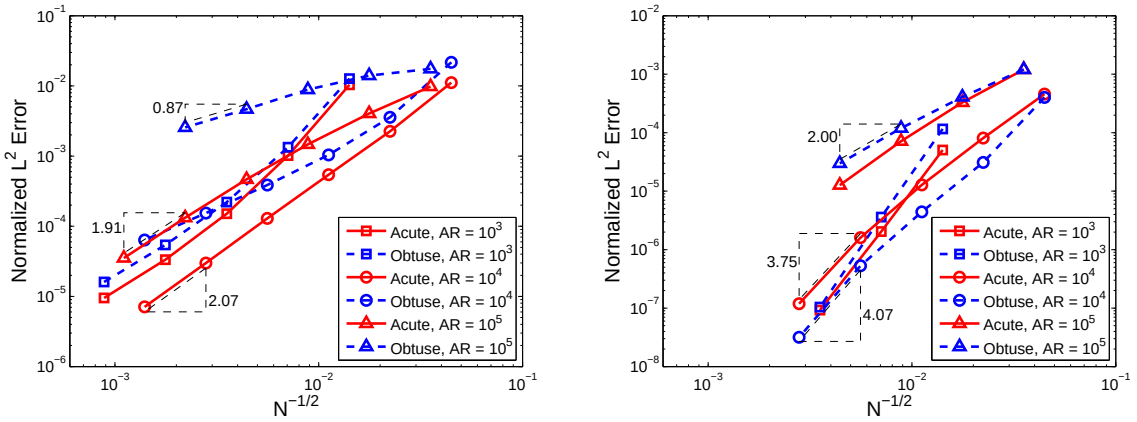

(a) Solution Order of $k = 1$ (b) Solution Order of $k = 3$

Fig. 8. Normalized L^2 error of ρu for the Navier-Stokes equations

Figure 9 shows the normalized output error for the acute and obtuse meshes, where the output is selected to be drag on the bottom wall. For linear solutions, at the aspect ratios of 10^3 and 10^4, the obtuse and acute elements lead to similar error levels. However, at $\mathcal{AR} = 10^5$, the acute elements outperform the obtuse ones significantly, and in fact, this shape leads to the lowest error for linear solutions. This optimality of acute triangles is very fragile in the sense that the error significantly increases when the aspect ratio deviates from 10^5. In fact, as it decreases to 10^3, the acute elements become the shape with the highest error for linear solutions, and as it increases to 10^6, the error also significantly increases. While this result seems to agree with Shewchuk's conclusion about the fragile "superaccuracy" of the H^1-seminorm of interpolation error for acute linear elements [34], the same behavior is not observed for the heat error in the advection-diffusion problem as in Fig. 6. Interpolation theory seems insufficient to explain this difference between output errors of two different governing equations under the DG discretization applied. In fact, this "superaccuracy" is not observed for the L^2 discretization errors either, which are also related to the H^1-seminorm of interpolation error as discussed in Section 5.1. On the other hand, for the high-order solutions in Fig. 9, the obtuse elements lead to a similar error compared to the acute ones for any aspect ratio, and the best triangle shape

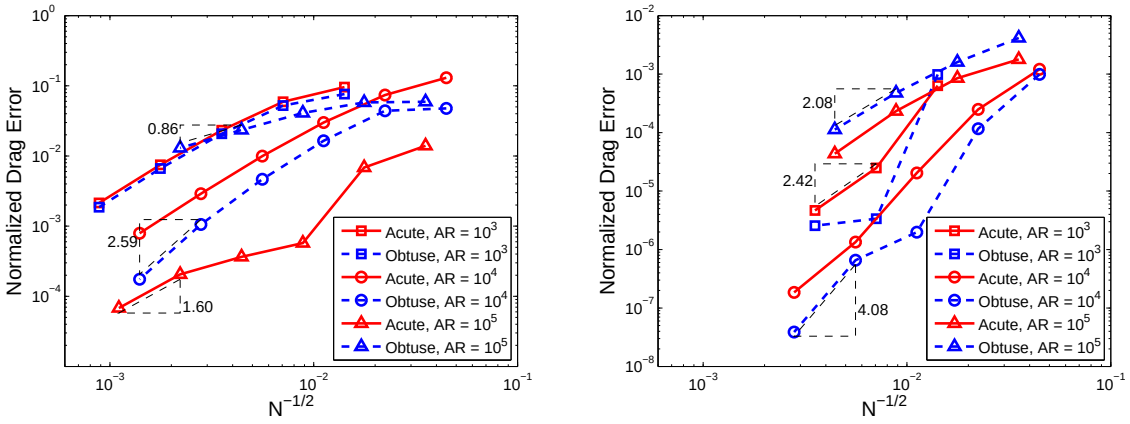

(a) Solution Order of $k = 1$ (b) Solution Order of $k = 3$

Fig. 9. Normalized drag error for the Navier-Stokes equations

is the obtuse ones with $\mathcal{AR} = 10^4$. Furthermore, for drag error, the impact of aspect ratio is again very pronounced for both linear and high-order solutions and for both element shapes.

Not only have the high-order solutions been shown to be less sensitive to element angles, the use of high-order schemes can also be justified from the perspective of the degrees of freedom needed for an error level. Figure 10 presents the worst and best output errors from the linear solutions and the high-order solutions from Fig. 9. Clearly, the high-order solutions lead to a lower error for almost all degrees of freedom for this problem. To put the error of drag in context, consider for example a typical large, long-range, passenger jet, an error of 1% for drag translates into approximately 4-8 passengers, depending on whether the configuration is limited by fuel volume or weight [16,36]. Thus, for the two-dimensional boundary layer problem studied, an output error level of $0.01\% - 1\%$ is a realistic range. Looking at this error range, all the meshes considered can reach this level with the high-order discretization. However, the best linear solution, which is obtained only on the acute meshes at a very sensitive optimal aspect ratio, can barely compete with the worst $k = 3$ solution. Therefore, higher-order discretizations are generally more efficient at achieving required error levels than their lower-order counterparts for sufficiently smooth flows.

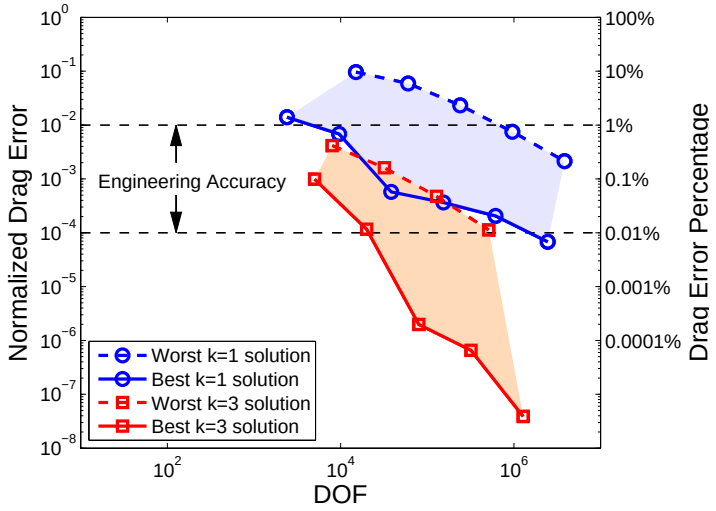

Fig. 10. Normalized drag error versus DOF for the Navier-Stokes equations

In practice, obtuse elements are often obtained from unstructured simplex mesh generation techniques, for example, a Delaunay triangulation in a stretched space, which is often applied in an adaptive setting for anisotropic problems. Thus, investigating the performance on unstructured meshes from these techniques has more practical values. The same model problem is studied on a series of unstructured meshes, generated from the Bi-dimensional Anisotropic Mesh Generator (BAMG), which is a Delaunay-type triangulator taking as an input metric tensors defined on a background mesh [7]. Figure 11 shows an example mesh, generated based on the metric tensor field of the obtuse mesh in Fig. 4. The definition of metric tensor can be found, for example, in [20,37].

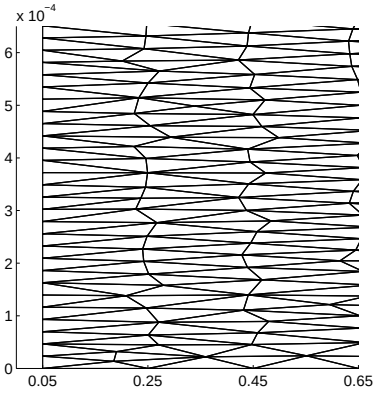

Fig. 11. Unstructured meshe

The error levels obtained on the unstructured meshes are essentially the same as those on the obtuse meshes for all the aspect ratios considered and for both solution orders. Figure 12 shows the worst and best drag errors on the unstructured meshes of different aspect ratios. The figure also includes the results from Fig. 10 for comparison.

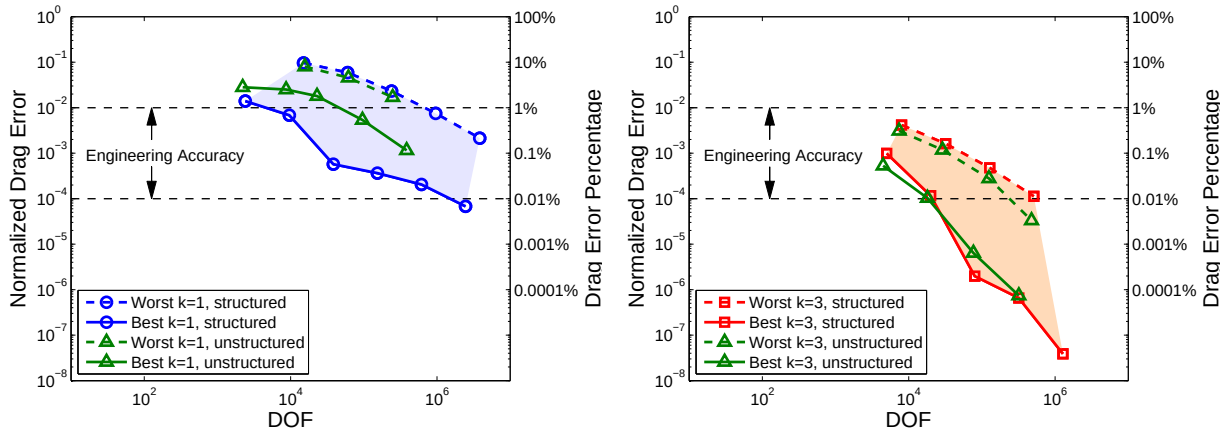

(a) Solution Order of $k = 1$

(b) Solution Order of $k = 3$

Fig. 12. Normalized drag error for the Navier-Stokes equations on structured and unstructured meshes

6. Conditioning of the Linear System

One important concern of the large-angle elements is their numerical conditioning, which impacts the efficiency of the iterative linear solvers applied. This section compares the conditioning of the linear systems

obtained from the acute and obtuse meshes, and studies the efficiency of the incomplete LU preconditioning for these meshes. The Jacobian matrix defined in Eq. (5) will still be denoted by $\mathbf{K}$, and $\mathbf{M}$ will denote the mass matrix defined by $\mathbf{M}_{ij} = \int_\Omega \boldsymbol{\phi}_i^T \boldsymbol{\phi}_j d\mathbf{x}$, where $\{\boldsymbol{\phi}_i\}$ is the basis for the function space $\mathcal{V}_H^p$ defined in Section 2.

6.1. *Eigenvalue Spectrum*

All eigenvalue calculations in this section are for the advection-diffusion problem. Table 1 compares the ratios of the maximum and minimum (by moduli) eigenvalues of $\mathbf{M}^{-1}\mathbf{K}$ from the acute and obtuse meshes. For all the aspect ratios considered, the acute and obtuse meshes have similar conditioning.

Table 1
Eigenvalues of $\mathbf{M}^{-1}\mathbf{K}$

Mesh	k	$\hat{\kappa} \equiv \lambda_{\max}/\lambda_{\min}$		
		$\hat{\kappa}_{\text{acute}}$	$\hat{\kappa}_{\text{obtuse}}$	$\hat{\kappa}_{\text{obtuse}}/\hat{\kappa}_{\text{acute}}$
$\mathcal{AR} = 10^3$, 512 elements	1	12.6	8.3	0.66
	3	97.2	75.4	0.77
$\mathcal{AR} = 10^4$, 500 elements	1	263.1	386.2	1.47
	3	1241.3	1746.0	1.41
$\mathcal{AR} = 10^5$, 800 elements	1	10365.1	16590.9	1.60
	3	48448.4	60505.5	1.25

Figure 13 shows the spectra for meshes of $\mathcal{AR} = 10^4$. The spectrum of $\mathbf{M}^{-1}\mathbf{K}$ is a measure of the ellipticity of the underlying problem and is independent of the type of interpolation basis chosen. Clearly, the problem is diffusion dominated as the eigenvalues are mainly real. In addition, the spectra for other aspect ratios indicate that the contribution of the diffusion term becomes more important as the aspect ratio increases, i.e., as the element y-spacing decreases while keeping about the same number of elements. Details can be found in [35].

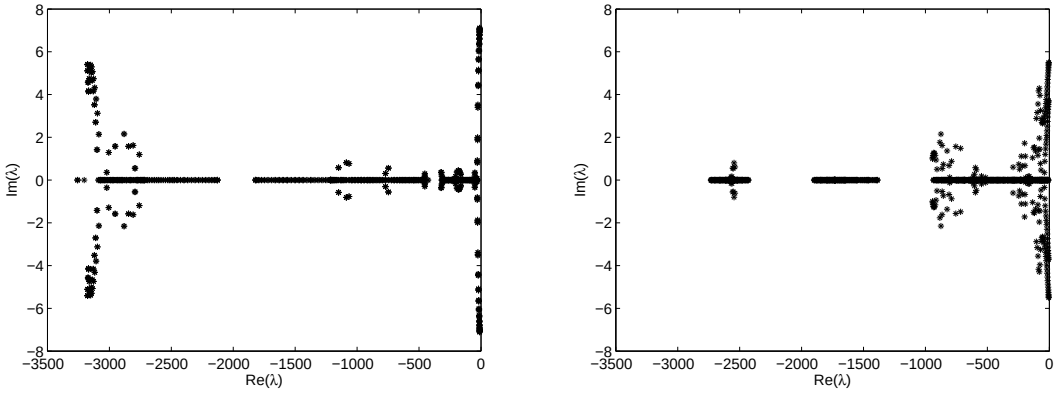

(a) Acute, $\mathcal{AR} = 10^4$, 500 elements

(b) Obtuse, $\mathcal{AR} = 10^4$, 500 elements

Fig. 13. Spectra of $\mathbf{M}^{-1}\mathbf{K}$ using linear interpolation

Another way to compare the conditioning is to look at the eigenvalue distributions of the block-Jacobi preconditioned system, $\mathbf{D}^{-1}\mathbf{K}$, where $\mathbf{D}$ is the block diagonal of $\mathbf{K}$. The spectrum is expected to fall in the unit circle centered at $(-1, 0)$, and as high-frequency errors can be removed fairly easily through preconditioning, the smallest eigenvalue (by moduli) implies the difficulty in solving the system. Table 2

lists the smallest eigenvalues for different meshes, and it confirms that the acute and obtuse elements have similar conditioning.

Table 2
Eigenvalues of block-Jacobi preconditioned $\mathbf{K}$

Mesh	k	$\hat{\lambda} \equiv \lambda_{\min}$		$\hat{\kappa} \equiv \lambda_{\max}/\lambda_{\min}$		
		$\hat{\lambda}_{\text{acute}}$	$\hat{\lambda}_{\text{obtuse}}$	$\hat{\kappa}_{\text{acute}}$	$\hat{\kappa}_{\text{obtuse}}$	$\hat{\kappa}_{\text{obtuse}}/\hat{\kappa}_{\text{acute}}$
$\mathcal{AR} = 10^3$, 512 elements	1	0.21	0.24	8.5	7.3	0.86
	3	0.072	0.096	26.9	19.9	0.74
$\mathcal{AR} = 10^4$, 500 elements	1	0.016	0.010	121.1	193.7	1.60
	3	0.0076	0.0059	262.4	338.9	1.29
$\mathcal{AR} = 10^5$, 800 elements	1	0.00042	0.00032	4714.9	6237.1	1.32
	3	0.00021	0.00024	9294.1	8179.0	0.88

6.2. *Preconditioning Strategies*

Although the conditioning of the linear systems arising from the two meshes is similar, comparing preconditioned systems has a more practical value as Krylov subspace methods must be preconditioned to perform well. This section studies the performance of ILU(0) and the more general ILUT(p, τ) on both the acute and the obtuse meshes for the linear systems defined in Eq. (5). Because the previous section has concluded that high-order discretization is preferred, only the preconditioning for the $k = 3$ discretization will be studied. For all the results in this section, the linear solver is iterated until the preconditioned residual reaches 10^{-14} relative to the initial residual.

6.2.1. *Performance of ILU(0)*

A sufficient condition for ILU(0) being the same as an exact factorization is that the linear system being solved is tridiagonal. For the Jacobian matrix arising from the presented DG discretization, this condition is equivalent to the following:

Tridiagonal Condition Each element on the mesh has no more than two neighbors with non-zero coupling.

This condition is equivalent to being able to partition the mesh into independent lines, where within each line, each element has only two neighbors. In practice, this can be rarely met. However, ILU(0) can work very efficiently with an appropriate reordering if a mesh is close to satisfying this condition, i.e., some elements might have a third neighbor with weak coupling instead of zero coupling.

For diffusion-dominated problems, the Tridiagonal Condition is generally far from being satisfied due to the typically isotropic nature of diffusion, which usually leads to strong couplings between all neighboring elements. However, for highly anisotropic meshes and/or convection-dominated problems, coupling in one direction can be much weaker than in another. As such, with an appropriate ordering of unknowns, ILU(0) works efficiently on the acute meshes for the model problem studied. Recall in this work that a Minimum Discarded Fill ordering is used such that discretizations that are close to satisfying the Triangular Condition should be effectively preconditioned by ILU(0). Table 3 lists the number of GMRES iterations using ILU(0) for acute and obtuse meshes of different aspect ratios. As shown in the table, ILU(0) works poorly for obtuse meshes, and as aspect ratio increases (i.e. as the contribution of diffusion becomes more important), the efficiency of ILU(0) drops quickly on these meshes. This can be explained by the strength of coupling between neighboring elements, which governs the performance of ILU(0).

Table 3
GMRES iteration counts using ILU(0) for the model advection-diffusion problem on different meshes

$\mathcal{R} = 10^3$, 512 elem.		$\mathcal{R} = 10^4$, 500 elem.		$\mathcal{R} = 10^5$, 800 elem.	
Acute	Obtuse	Acute	Obtuse	Acute	Obtuse
16	29	6	50	4	183

Let the coupling weight for an element κ with its neighbor κ' be the corresponding entry in $\mathbf{K}$ normalized by the diagonal entry for κ, that is, $\eta_{\kappa\kappa'} \equiv \mathbf{K}_{\kappa\kappa'}/\mathbf{K}_{\kappa\kappa}$, where $\mathbf{K}_{ij}$ denotes the ij block in the matrix $\mathbf{K}$ measured in a certain norm, for example, the Frobenius norm.

For a diffusion-dominated problem, the coupling weight $\eta_{\kappa\kappa'}$ scales with $(l_f/d_\kappa)^2$, where l_f is the length of the face between κ and κ', and d_κ is a measure of the diameter of the element κ. This is demonstrated in Appendix through an order analysis. A highly anisotropic right triangle has one edge much shorter than the other two, and so for the model problem considered, the coupling weight on this short edge is negligible. Thus, the acute meshes are close to satisfying the Tridiagonal Condition. Furthermore, as the aspect ratio increases, the short edge becomes even shorter, and the coupling across this edge becomes even more insignificant, making ILU(0) perform even better. This is consistent with the results in Table 3. On the other hand, an obtuse triangle does not have this property as all its three edges have similar lengths. This is illustrated in Fig. 14. As the diffusion term becomes more important, the coupling across each edge on the obtuse meshes becomes stronger. Conversely, if less diffusion were introduced such that the problem became advection dominated, ILU(0) would work equally well on the acute and the obtuse meshes.

In summary, for ILU(0), the key factor for efficiency is not the maximum angle involved, but the connectivity weight with neighbors, or the strength of coupling among elements. If all three edges of one element have equal coupling strength, regardless of the largest angle involved, then the Tridiagonal Condition will be far from being satisfied, and ILU(0) will have difficulties working efficiently. In fact, for the same reason, ILU(0) works poorly for a simple diffusion-dominated problem on equilateral triangles, as reported by Persson [28].

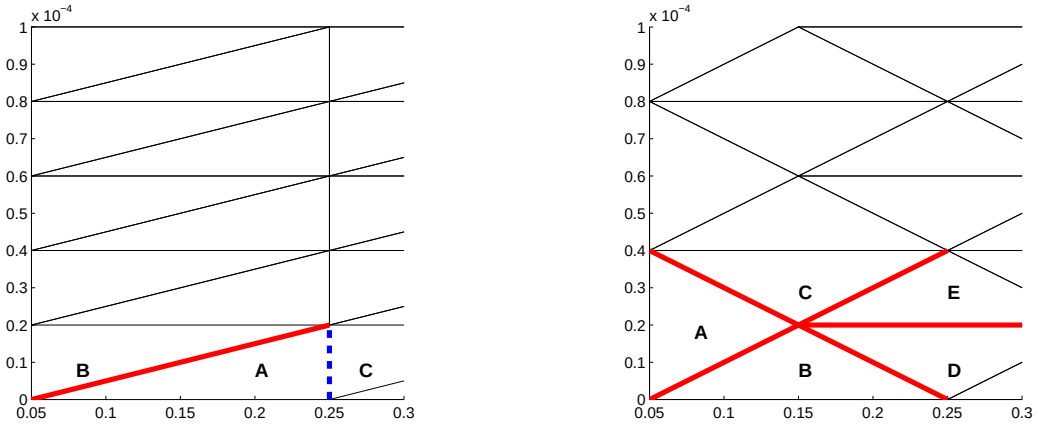

(a) Acute Elements (b) Obtuse Element

Fig. 14. Coupling weights for diffusion dominated problems. For acute elements, the dashed edge is much shorter than the solid one, so elimination of element A will not introduce a significant fill-in between elements B and C. However, for obtuse elements, all edges have similar length and thus similar connectivity weight, elimination of any element will introduce a large fill-in.

To further demonstrate that angle size by itself is not a determining factor in the efficiency of ILU(0), two diffusion cases with anisotropic diffusivity tensors are presented. Both cases use the meshes of $\mathcal{R} = 10^4$ with 500 elements. An analysis of coupling weights for anisotropic diffusion can be found in [35].

The first case is a pure diffusion problem with a diffusivity tensor given by

$$\bar{\bar{\mu}} = \begin{bmatrix} 1 \times 10^{-8} & 2 \times 10^{-12} \\ 2 \times 10^{-12} & 4 \times 10^{-16} \end{bmatrix}. \tag{9}$$

With this diffusivity, the diffusion is zero across one edge of each element on the obtuse meshes, and the coupling is shown in Fig. 15.

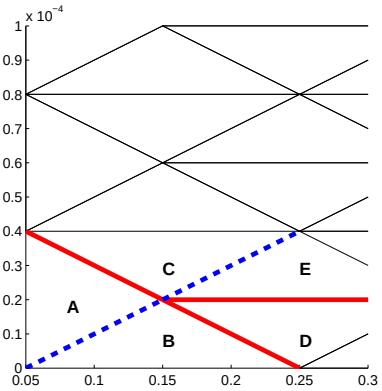

Fig. 15. Coupling weights for the anisotropic diffusivity in Eq. (9) on the obtuse meshes. The coupling is zero across the dashed edges, so elimination of element A will not introduce any fill-in between elements B and C.

Table 4 lists the ratio of maximum and minimum eigenvalues, $\lambda_{\max}/\lambda_{\min}$, for the unpreconditioned system, $\mathbf{M}^{-1}\mathbf{K}$, and also the number of GMRES iterations for the ILU(0) preconditioned system with the MDF reordering. As the table shows, although the system for the obtuse mesh is conditioned only a little better than that for the acute one, ILU(0) works very efficiently for the obtuse mesh as argued based on the strength of coupling among elements.

Table 4
Performance of ILU(0) for anisotropic diffusion in Eq. (9) on meshes of $\mathcal{AR} = 10^4$, 500 elements

$\lambda_{\max}/\lambda_{\min}$ of $\mathbf{M}^{-1}\mathbf{K}$		GMRES It. with ILU(0)	
Acute	Obtuse	Acute	Obtuse
9.44×10^4	5.69×10^4	81	1

The second case has a diffusivity tensor given by

$$\bar{\bar{\mu}} = \begin{bmatrix} 10^{-8} & 0 \\ 0 & \mu \end{bmatrix}, \tag{10}$$

where μ controls the diffusivity in the y-direction. As it decreases, the relative importance of the diffusivity in the x-direction increases, and so the coupling strength across the short edges on the acute meshes increases.

Table 5 lists $\lambda_{\max}/\lambda_{\min}$ for the unpreconditioned system, and also the number of GMRES iterations for the ILU(0) preconditioned system. As less diffusion is introduced in the y-direction, the unpreconditioned system becomes better conditioned. However, ILU(0) works less efficiently as the three edges of each element become equally weighted.

6.2.2. *Preconditioning on Obtuse Meshes*

Knowing that ILU(0) works efficiently for the acute meshes (when appropriately aligned), it is desirable to develop an equally efficient preconditioner for the obtuse meshes. h- and/or p-multigrid preconditioners are known to work well for diffusion-dominated problems, and they have been applied in a DG context [28,18,24]. However, in this work, the ILUT(p,τ) is considered for the obtuse meshes, and its efficiency is compared with the ILU(0) results on the acute and obtuse meshes.

Table 5
Performance of ILU(0) for anisotropic diffusion in Eq. (10) on acute mesh of $\mathcal{R} = 10^4$, 500 elements

μ	$\lambda_{\max}/\lambda_{\min}$ of $\mathbf{M}^{-1}\mathbf{K}$	GMRES It. with ILU(0)
10^{-8}	3.12×10^5	3
10^{-12}	3.11×10^5	30
10^{-16}	2.14×10^4	74

A fill-in level of two is considered in this work and is found to be temporally more efficient than a level of one. A higher level is deemed to be too expensive due to memory concerns. Table 6 lists the ILU(0) and ILUT results for the acute and obtuse meshes. As shown in the table, ILU(0) works poorly for the obtuse meshes as explained previously. The ILUT preconditioner results in a significant improvement. For the Navier-Stokes equations, the computational cost on the obtuse meshes using ILUT is comparable to that on the acute meshes using ILU(0). Also, as ILU(0) works very efficiently on the acute meshes, ILUT does not lead to an obvious improvement on these meshes, especially for the advection-diffusion equation. Thus, ILUT results on the acute meshes are not included.

Table 6
Comparison of preconditioned systems for acute and obtuse meshes[a]

Mesh	Preconditioner	Advection-Diffusion Equation		Navier-Stokes Equations[b]	
		GMRES Iter.	Time[c]	GMRES Iter.	Time[c]
Acute	ILU(0)	6	0.108	86	2.977
Obtuse	ILU(0)	50	0.324	188	7.309
Obtuse	ILUT[d]	11	0.173	69	3.267

[a] $\mathcal{R} = 10^4$, 500 elements. Solution order $k = 3$.
[b] Linear system from the converged solution state.
[c] Total wall clock time of the linear solver including reordering, factorization, and GMRES, measured on an Intel Xeon 5130 processor at 2.00GHz. O/S: Red Hat Enterprise Linux 4.
[d] ILUT with a fill-in level of two and a threshold of $\tau = 10^{-6}$.

Let the wall clock time of the linear solve using ILU(0) on the acute meshes be $t_a \equiv t_a^{\text{fac}} + t_a^{\text{GMRES}}$, where t_a^{fac} denotes the factorization time and t_a^{GMRES} is the GMRES time. Similarly, let the wall clock time of the linear solve using ILUT on the obtuse meshes be $t_o \equiv t_o^{\text{fac}} + t_o^{\text{GMRES}}$. Figure 16 plots the ratio of t_o/t_a versus different drop thresholds for ILUT with a fill-in level of two. With a value of $\tau = 10^{-6}$, t_o is about 60% higher (i.e. slower) than t_a for the advection-diffusion equation. However, it is about 15% higher for the Navier-Stokes equations, for which more complicated characteristics and element-to-element couplings are involved compared to the advection-diffusion equation. To further illustrate, Fig. 17 shows the ratio of $t_o^{\text{fac}}/t_a^{\text{fac}}$ and $t_o^{\text{GRMES}}/t_a^{\text{GMRES}}$ for the two equations. As seen, the factorization time ratio, $t_o^{\text{fac}}/t_a^{\text{fac}}$, is significantly higher for the Navier-Stokes equations as bigger matrix block sizes are involved. On the other hand, the GMRES time ratio, $t_o^{\text{GRMES}}/t_a^{\text{GMRES}}$, is higher for the advection-diffusion equation as the number of GMRES iterations using ILU(0) is very small for this equation on the acute meshes. Since GMRES time is dominant in the total linear solver time, the difference between t_a and t_o is much smaller for the Navier-Stokes equations than for the advection-diffusion equation. Also, note that for each of the model equations, there is a critical value of τ, above which the GMRES time significantly increases, indicating that important information is dropped in the factorization stage.

6.3. *Discussion*

For three-dimensional problems, the Tridiagonal Condition is still a sufficient condition for ILU(0) to be exact factorization, with an appropriate ordering regardless of the element angles involved. Further, consider an acute tetrahedron with a single short edge, and an obtuse tetrahedron in which all edges are of similar length but the height of the tetrahedron is much smaller. Then the acute tetrahedron has two faces much

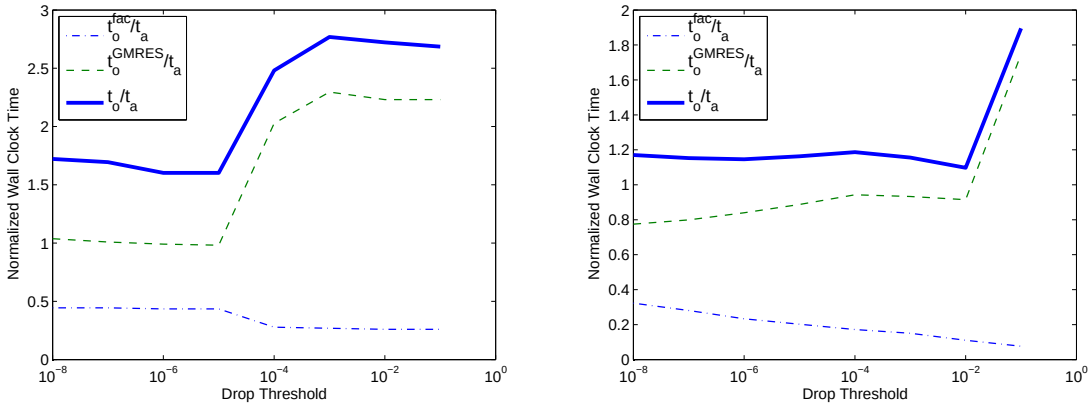

(a) Advection-diffusion equation

(b) Navier-Stokes equations

Fig. 16. Wall clock time for linear solver using ILUT on obtuse mesh normalized by the linear solver time using ILU(0) on acute mesh of 500 elements at $\mathcal{AR} = 10^4$

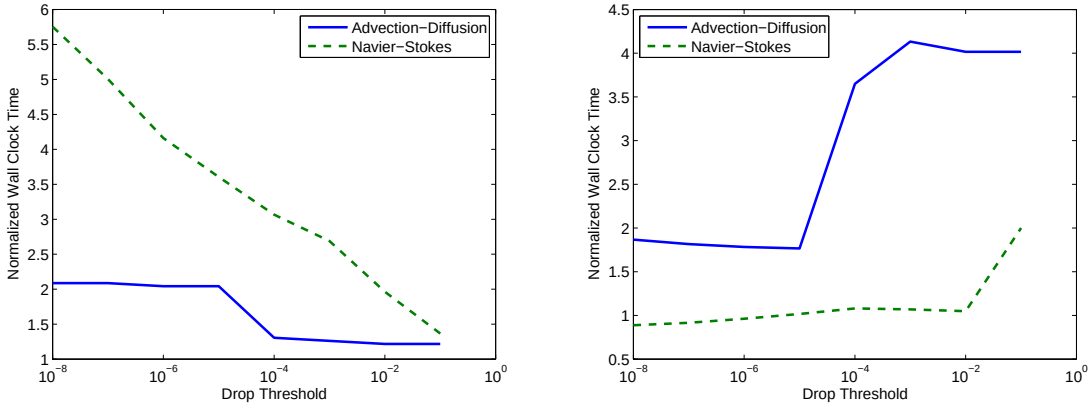

(a) Factorization time, $t_o^{\text{fac}}/t_a^{\text{fac}}$

(b) GMRES time, $t_o^{\text{GMRES}}/t_a^{\text{GMRES}}$

Fig. 17. Factorization time and GMRES time using ILUT on obtuse mesh normalized by the corresponding time using ILU(0) on acute mesh of 500 elements at $\mathcal{AR} = 10^4$

smaller than the other two, making the mesh very close to satisfying the Tridiagonal Condition. Hence, ILU(0) will work very efficiently on this mesh for an isotropic diffusion problem. On the other hand, the tetrahedra from the obtuse triangle will have all faces of similar areas, and so similar coupling strengths with neighbors. This will lead to a poor performance of ILU(0). In addition, ILUT might not be as efficient as in two-dimension because more off-diagonal blocks are present in each row of the Jacobian matrix.

The conclusion about ILU(0) for the acute and obtuse elements is valid for a discretization with a nearest-neighbor stencil or a discretization with the nearest-neighbor coupling much stronger than farther-neighbor coupling. Such discretization includes, for example, a DG discretization with BR2 for the diffusion term [5], or a Compact DG method [26]. On the other hand, ILU(0) may be a poor preconditioner, even on the acute elements, for a discretization with more complicated coupling. For example, a standard Galerkin method has neighbor coupling defined among nodes, making ILU(0) less efficient than for a DG method.

7. Conclusion

In this work, the impact of triangle shapes, including large angles and aspect ratios, on accuracy and stiffness for simulations of highly anisotropic problems has been studied. With a high-order DG discretization,

it is seen that the discretization error is not sensitive to the maximum angles involved, but using a correct aspect ratio is critical. In addition, the linear system induced from obtuse meshes has similar conditioning with that from acute meshes. However, the solution schemes for these two meshes differ as they involve different coupling strengths among elements. For this reason, ILU(0) has been shown less efficient on obtuse meshes for an isotropic diffusion problem. With an ILUT preconditioner, the solution on obtuse meshes can be achieved within a comparable time as on acute meshes. Therefore, for anisotropic meshing with high-order discretizations, while aspect ratio is critical, large angles can be overcome through small increases in preconditioning costs.

Acknowledgments

The authors would like to thank the Project X development team for the many contributions. This work was partially supported by funding from The Boeing Company with technical monitor Dr. Mori Mani.

Appendix

This appendix derives the scaling of the coupling weights in the Jacobian matrix arising from the applied DG discretization for a diffusion problem with isotropic diffusivity. The derivation is for one interior element, κ, with its neighbor, κ', as shown in Fig. 18. The derivation for other neighbors is similar. Denote the face between κ and κ' by σ_f, whose the normal vector is $\hat{\mathbf{n}} = [1, 0]^T$.

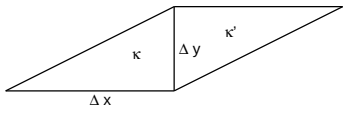

Fig. 18. Example element for deriving the scaling of coupling weights in Jacobian matrix

The residual for this problem is given by

$$\mathcal{R}_{H\kappa}(\mathbf{u}_H, \mathbf{v}_H) = \underbrace{\int_\kappa \nabla \mathbf{v}_H^T \cdot \mu \nabla \mathbf{u}_H d\mathbf{x}}_{\text{Term } I} + \underbrace{\int_{\partial\kappa} (\nabla \mathbf{v}_H^T)^+ \left(\widehat{\mu \mathbf{u}} - \mu^+ \mathbf{u}_H^+\right) \cdot \hat{\mathbf{n}} ds}_{\text{Term } II} - \underbrace{\int_{\partial\kappa} \mathbf{v}_H^+ \hat{\mathcal{Q}} \cdot \hat{\mathbf{n}} ds}_{\text{Term } III}, \tag{11}$$

where $\widehat{\mu \mathbf{u}} = \mu^+ \{\mathbf{u}_H\}$, $\hat{\mathcal{Q}} = \{\mu \nabla \mathbf{u}_H\} - \eta_f \{\boldsymbol{\delta}_f\}$, and η_f is a specified stabilization parameter. The notations $()^+$ and $()^-$ refer to data on the interior and exterior of an element boundary, respectively. The auxiliary variables $\boldsymbol{\delta}_f \in \left(\mathcal{V}_H^p\right)^d$ are defined such that

$$\int_\kappa \boldsymbol{\tau}_H^T \cdot \boldsymbol{\delta}_{f\kappa} d\mathbf{x} + \int_{\kappa'} \boldsymbol{\tau}_H^T \cdot \boldsymbol{\delta}_{f\kappa'} d\mathbf{x} = \int_{\sigma_f} [\![\mathbf{u}_H]\!]^T \cdot \{\mu \boldsymbol{\tau}_H\} ds, \quad \forall \boldsymbol{\tau}_H \in \left(\mathcal{V}_H^p\right)^d. \tag{12}$$

The operators $\{\cdot\}$ and $[\![\cdot]\!]$ denote average and jump operators, respectively.

The discrete residual vector is given by $\mathbf{R}_H(\mathbf{U}_H)_\kappa = \mathcal{R}_H(\mathbf{u}_H, \boldsymbol{\phi}_\kappa)$ for the element κ, where $\boldsymbol{\phi}_\kappa$ is the set of all basis functions with support in κ, and $\mathbf{u}_H(\mathbf{x})\big|_\kappa = \mathbf{U}_H^T\big|_\kappa \boldsymbol{\phi}_\kappa$. The Jacobian matrix, $\mathbf{K} = \frac{\partial \mathbf{R}_H}{\partial \mathbf{U}_H}$, involves differentiating each term in Eq. (11) with respect to $\mathbf{U}_H$. To derive the scaling of these terms, assume for each basis function $\boldsymbol{\phi}$ that

$$\boldsymbol{\phi} \sim \mathcal{O}(1), \quad \nabla \boldsymbol{\phi} \sim \mathcal{O}\left(\left[\frac{1}{\Delta x}, \frac{1}{\Delta y}\right]^T\right). \tag{13}$$

From Eq. (12), one can derive the scaling of $\boldsymbol{\delta}_f$ to be $\boldsymbol{\delta}_f \sim \mathcal{O}([\frac{\Delta y}{A}|\mathbf{U}_H|, 0]^T)$, where $A = \frac{1}{2}\Delta x \Delta y$ is the element area, and $|\mathbf{U}_H|$ is a certain measure of the solution vector. Thus, the scaling of each term in Eq. (11) is found to be

$$\text{Term } I \sim \mathcal{O}\left(\mu\left(\frac{\Delta y}{\Delta x}+\frac{\Delta x}{\Delta y}\right)|\mathbf{U}_H|\right)$$
$$\text{Term } II \sim \mathcal{O}\left(\mu\frac{\Delta y}{\Delta x}|\mathbf{U}_H|\right)$$
$$\text{Term } III \sim \mathcal{O}\left(\mu\frac{\Delta y}{\Delta x}|\mathbf{U}_H|\right).$$

For the block row corresponding to κ in the matrix $\mathbf{K}$, the diagonal block $K_{\kappa\kappa}$ involves the derivatives of all the three terms, while the off-diagonal block $K_{\kappa\kappa'}$ has the derivatives of the terms II and III. Thus, with the blocks measured in a certain norm, the coupling weight of κ with κ' scales with

$$\frac{K_{\kappa\kappa'}}{K_{\kappa\kappa}} \sim \mathcal{O}\left(\frac{\frac{\Delta y}{\Delta x}}{\frac{\Delta y}{\Delta x}+\frac{\Delta x}{\Delta y}}\right) \sim \mathcal{O}\left(\frac{\Delta y^2}{\Delta x^2+\Delta y^2}\right). \tag{14}$$

In other words, the coupling scales with $\mathcal{O}\left(l_f/d_\kappa\right)^2$, where l_f is the length of the face between κ and κ', and d_κ is a measure of the diameter of the element κ.

References

[1] T. Apel, M. Dobrowolski, Anisotropic interpolation with applications to the finite element method, Computing 47 (1992) 277–293.

[2] D. N. Arnold, F. Brezzi, B. Cockburn, L. D. Marini, Unified analysis of discontinuous Galerkin methods for elliptical problems, SIAM J. Numer. Anal. 39 (5) (2002) 1749–1779.

[3] I. Babuška, A. K. Aziz, On the angle condition in the finite element method, SIAM J. Numer. Anal. 13 (2) (1976) 214–226.

[4] T. J. Barth, Numerical aspects of computing viscous high reynolds number flows on unstructured meshes, AIAA 1991-0721 (1991).

[5] F. Bassi, S. Rebay, GMRES discontinuous Galerkin solution of the compressible Navier-Stokes equations, in: K. Cockburn, Shu (eds.), Discontinuous Galerkin Methods: Theory, Computation and Applications, Springer, Berlin, 2000, pp. 197–208.

[6] M. Benzi, D. B. Szyld, A. van Duin, Orderings for incomplete factorization preconditioning of nonsymmetric problems, SIAM J. Sci. Comput. 20 (5) (1999) 1652–1670.

[7] H. Borouchaki, P. George, F. Hecht, P. Laug, E. Saltel, Mailleur bidimensionnel de Delaunay gouverné par une carte de métriques. Partie I: Algorithmes, INRIA-Rocquencourt, France. Tech Report No. 2741 (1995).

[8] H. Borouchaki, P. L. George, F. Hecht, P. Laug, E. Saltel, Delaunay mesh generation governed by metric specifications. Part I algorithms, Finite Elem. Anal. Des. 25 (1-2) (1997) 61–83.

[9] W. Cao, On the error of linear interpolation and the orientation, aspect ratio, and internal angles of a triangle, SIAM J. Numer. Anal. 43 (1) (2005) 19–40.

[10] W. Cao, Anisotropic measures of third order derivatives and the quadratic interpolation error on triangular elements, SIAM J. Sci. Comput. 29 (2) (2007) 756–781.

[11] W. Cao, An interpolation error estimate in $\mathcal{R}^2$ based on the anisotropic measures of higher order derivatives, Math. Comp. 77 (261) (2008) 265–286.

[12] E. F. D'Azevedo, P. A. Forsyth, W.-P. Tang, Ordering methods for preconditioned conjugate gradient methods applied to unstructured grid problems, SIAM J. Matrix Anal. Appl. 13 (3) (1992) 944–961.

[13] C. Dobrzynski, P. Frey, Anisotropic Delaunay mesh adaptation for unsteady simulations, in: 17th Intl. Meshing Roundtable, 2008, pp. 177–194.

[14] Q. Du, D. Wang, L. Zhu, On mesh geometry and stiffness matrix conditioning for general finite element spaces, SIAM J. Numer. Anal. 47 (2) (2009) 1421–1444.

[15] H. Edelsbrunner, T. S. Tan, R. Waupotitsch, An $o(n^2 \log n)$ time algorithm for the minmax angle triangulation, SIAM Journal on Scientific and Statistical Computing 13 (4) (1992) 994–1008.

[16] K. J. Fidkowski, A high-order discontinuous Galerkin multigrid solver for aerodynamic applications, Masters thesis, Massachusetts Institute of Technology, Department of Aeronautics and Astronautics (Jun. 2004).

[17] K. J. Fidkowski, D. L. Darmofal, A triangular cut-cell adaptive method for higher-order discretizations of the compressible Navier-Stokes equations, J. Comput. Phys. 225 (2007) 1653–1672.

[18] K. J. Fidkowski, T. A. Oliver, J. Lu, D. L. Darmofal, p-Multigrid solution of high-order discontiunous Galerkin discretizations of the compressible Navier-Stokes equations, J. Comput. Phys. 207 (1) (2005) 92–113.

[19] M. B. Giles, E. Süli, Adjoint methods for PDEs: a posteriori error analysis and postprocessing by duality, in: Acta Numerica, vol. 11, 2002, pp. 145–236.

[20] W. G. Habashi, J. Dompierre, Y. Bourgault, D. Ait-Ali-Yahia, M. Fortin, M.-G. Vallet, Anisotropic mesh adaptation: towards user-independent, mesh-independent and solver-independent CFD. part I: general principles, Internat. J. Numer. Methods Fluids 32 (2000) 725–744.

[21] Y. Kallinderis, K. Nakajima, Finite element method for incompressible viscous flows with adaptive hybrid grids, AIAA Journal 32 (8) (1994) 1617–1625.
[22] R. Löhner, Matching semi-structured and unstructured grids for Navier-Stokes calculations, AIAA 1993-3348 (1993).
[23] J. Lu, An a posteriori error control framework for adaptive precision optimization using discontinuous Galerkin finite element method, Ph.D. thesis, Massachusetts Institute of Technology, Cambridge, Massachusetts (2005).
[24] C. R. Nastase, D. J. Mavriplis, High-order discontinuous Galerkin methods using an *hp*-multigrid approach, J. Comput. Phys. 213 (1) (2006) 330–357.
[25] T. A. Oliver, Multigrid solution for high-order discontinuous Galerkin discretizations of the compressible Navier-Stokes equations, Masters thesis, Massachusetts Institute of Technology, Department of Aeronautics and Astronautics (Jun. 2004).
[26] J. Peraire, P.-O. Persson, The compact discontinuous galerkin (CDG) method for elliptic problems, SIAM J. Sci. Comput. 30 (4) (2008) 1806–1824.
[27] J. Peraire, M. Vahdati, K. Morgan, O. C. Zienkiewicz, Adaptive remeshing for compressible flow computations, J. Comput. Phys. 72 (1987) 449–466.
[28] P.-O. Persson, J. Peraire, Newton-GMRES preconditioning for discontinuous Galerkin discretizations of the Navier-Stokes equations, SIAM J. Sci. Comput. 30 (6) (2008) 2709–2722.
[29] S. Rippa, Long and thin triangles can be good for linear interpolation, SIAM J. Numer. Anal. 29 (1) (1992) 257–270.
[30] P. L. Roe, Approximate Riemann solvers, parameter vectors, and difference schemes, J. Comput. Phys. 43 (2) (1981) 357–372.
[31] Y. Saad, ILUT: a dual threshold incomplete LU factorization 1 (4) (1994) 387–402.
[32] Y. Saad, Iterative Methods for Sparse Linear Systems, Society for Industrial and Applied Mathematics, 1996.
[33] Y. Saad, M. H. Schultz, GMRES: A generalized minimal residual algorithm for solving nonsymmetric linear systems, SIAM Journal on Scientific and Statistical Computing 7 (3) (1986) 856–869.
[34] J. R. Shewchuk, What is a good linear finite element? Interpolation, conditioning, anisotropy, and quality measures, Tech. rep., University of California at Berkeley (2002).
[35] H. Sun, Impact of triangle shapes using high-order discretizations and direct mesh adaptation for output error, Masters thesis, Massachusetts Institute of Technology, Computation for Design and Optimization Program (2009).
[36] J. C. Vassberg, M. A. DeHaan, T. J. Sclafani, Grid generation requirements for accurate drag predictions based on OVERFLOW calculations, AIAA 2003-4124 (2003).
[37] D. A. Venditti, D. L. Darmofal, Anisotropic grid adaptation for functional outputs: Application to two-dimensional viscous flows, J. Comput. Phys. 187 (1) (2003) 22–46.